International Journal of Heat and Mass Transfer 52 (2009) 1167–1176

Contents lists available at ScienceDirect

International Journal of Heat and Mass Transfer

journal homepage: www.elsevier.com/locate/ijhmt

Multi-objective genetic optimization of the heat transfer from longitudinal wavy fins

Diego Copiello [a,*], Giampietro Fabbri [b]

[a] Università di Bologna Seconda Facoltà di Ingegneria, via Fontanelle 40, 47100 Forlì, Italy
[b] Dipartimento di Ingegneria Energetica Nucleare e del Controllo Ambientale, Università di Bologna, Via Zannoni 45/2, 40134 Bologna, Italy

ARTICLE INFO

Article history:
Received 5 November 2007
Available online 7 November 2008

Keywords:
Fins
Genetic algorithms
Multi-objective optimization

ABSTRACT

In the present work, we investigate the optimization of the heat transfer from wavy fins cooled by a laminar flow under conditions of forced convection and from a multi-objective point of view. The problem is addressed by means of a finite element method which allows to compute the velocity and the temperature distributions in a finned conduit cross section under conditions of imposed heat flux. Thereafter, the fin profile is optimized by means of multi-objective genetic algorithm which aims to find geometries that maximize the heat transfer and, at the same time, minimize the hydraulic resistance. The geometry of the fins is parameterized by means of a polynomial function and several order are investigated and compared.

© 2008 Elsevier Ltd. All rights reserved.

1. Introduction

In many engineering fields, finned dissipators are an invaluable tool to remove heat in particular where high fluxes must be transferred. A typical use of such a heat exchanger can be found in the electronic industry where components must be cooled in order to ensure both performance and reliability. Moreover, the temperature of an electronic component must be lowered considering also the exigence of reducing the energy consumption of cooling fans and reducing the volume of the device. For example, the former exigence is connected with the customer requirement of long battery endurance. Whereas, the latter exigence is related to the weight and to the volume of the device. In recent years in fact, the electronic industry has developed smaller and smaller components and the heat dissipators for them must consequently be scaled. Another reason that lead to the reduction of the finned dissipator volume is the necessity of lowering the amount of material used in the device. In fact, as reported by the LCA Committee of the Japanese aluminum industry [1] and recalled by Bar-Choen and Iyengar [2], the estimated amount of aluminium used for cooling electronic devices was of about 10 Million-kg in 2001. Although, we have focused only in the electronic field so far, similar considerations can be easily made in all fields were heat dissipators play a fundamental role.

The problem of the optimization of longitudinal fins has been studied by many researchers in the last century [3–6]. In particular several fin profiles have been suggested and undulated fins have shown the best performances in terms of heat transfer [8,7]. However, the optimum fin shape has been solved only partially. In fact, a criterion for detecting the optimal geometry has been proposed by Fabbri [9,10] where a genetic algorithm has been employed to detect the geometry that ensures the highest heat transfer. However, as just pointed out the optimum geometry itself may not be useful since limits in the hydraulic resistance or in the volume of the fins may also arise. Although, the genetic algorithm previously used can be employed considering constraints in the hydraulic resistance, the value of such limits is typically unknown *a priori*. Hence, a different approach should be used and in this case *multi-objective optimization* techniques are suitable methods since their application together with genetic algorithms permits to detect rapidly the set of solutions that optimize all the objectives of interest.

Although, these techniques have been developed since the mid-1980s, their usage in the heat transfer field is recent and not common. In particular, Hilbert et al. [11] performed a multi-objective shape design optimization of a tube bank heat exchanger whereas, Nobile et al. [12] studied convective periodic channels.

In the present work, we investigate the optimization of heat transfer through finned dissipators by means of a multi-objective genetic algorithm where the two objectives considered here are the maximization of the heat transfer and, at the same time, the minimization of the hydraulic resistance. Since the two objectives are conflicting, the result of the genetic algorithm is a set of optimal solutions each of them lying on a trade-off curve called Pareto front. The same methodology is then applied considering different constraints in the volume of the fins. Finally, we want to investigate how the irreversibility of the heat transfer and fluid flow processes influences the geometries lying on the trade-off curve. Specifically, this last analysis is carry out by minimizing the entropy generation rate and maximizing the heat transfer.

* Corresponding author. Tel.: +39 543 37449; fax: +39 543 374444.
E-mail address: diego.copiello@unibo.it (D. Copiello).

0017-9310/$ - see front matter © 2008 Elsevier Ltd. All rights reserved.
doi:10.1016/j.ijheatmasstransfer.2008.09.012

Nomenclature

a	fin height (m)
b	fin base thickness (m)
c_p	specific heat of the coolant (J/kg K)
D	individual density
d	distance between the fin base thickness and the opposite flat wall (m)
e	width of the portion of conduit section (m)
F	individual fitness
f	half-width of the fins (m)
h	global heat transfer coefficient (W/m^2 K)
k_c	thermal conductivity of the coolant (W/mK)
k_f	thermal conductivity of the finned plate (W/mK)
N	population size
n	polynomial order
Nu_e	equivalent Nusselt number
p	generalized pressure (N/m^2)
q''	heat flux per unit surface uniformly imposed on the finned plate (W/m^2)
R	individual raw fitness
S	individual strength
T_b	bulk temperature of the coolant (K)
T_c	temperature of the coolant (K)
T_f	temperature of the finned plate (K)
T_{max}	maximum temperature of the cooled surface (K)
u	velocity of the coolant (m/s)
w_t	total coolant volume flow rate (m^3/s)
x	longitudinal coordinate (m)
y	coordinate parallel to fin height (m)
z	coordinate orthogonal to fin height (m)

Greek symbols

α	normalized height of the fins, a/d
β	normalized thickness of the finned plate base, b/d
ϵ	normalized width of the portion of conduit section, e/d
η	normalized coordinate parallel to fin height, y/d
γ	ratio of finned plate to coolant conductivity, k_f/k_c
μ	dynamic viscosity (Pa s)
ϕ	normalized half-width of the fins, f/d
ϕ_i	fin profile describing parameters
ψ_i	polynomial coefficients
ρ	coolant density (kg/m^3)
ζ	normalized hydraulic resistance, defined by Eq. (6)

2. Governing equations and dimensioning criteria

Let us consider a conduit composed by a finned plate opposite to a flat surface, both of them infinitely long and wide. The flat surface is thermally insulated while a constant heat flux q'' is applied to the finned plate bottom. The coolant flows in the conduit parallel to the fins. All conduit fins are identical and the sections orthogonal to the flow direction have two symmetry axes (see Fig. 1).

Since the present work considers an optimization technique that employs a large number of individuals in order to correctly solve the problem, the simplicity of the model is mandatory. In fact, for the test cases considered (cf. Section 4) a population of 100 individuals that reproduces for 100 generations have to be considered in order to detect the real Pareto front. Therefore, a total number of 10000 cost functions evaluations is required. For such a large number of individuals, the usage of time consuming solvers is not allowed in order to obtain results within a reasonable time. For this reason, in the present work we introduce the following hypotheses and considerations:

- the fluid flow is laminar and incompressible;
- the system is in steady state;
- velocity and temperature are fully developed;
- fluid and solid properties are uniform and fluid independent;
- natural convection is negligible in regard to the forced convection;
- viscous dissipation is negligible.

The heat transfer performance of the system can be studied considering only a portion of it which is delimited by the finned plate bottom, the top flat surface, and two symmetry axes (see Fig. 2). Let us choose an orthogonal coordinate system where the x axis is parallel to the streamwise direction, the y axis is perpendicular to the flat plate while the z direction is parallel to it. As shown in Fig. 2, let a be the fin height, b the fin base thickness, e the distance between the two symmetry axes, and d the distance between the fin base and the flat surface.

Under such conditions, only the x component u of the fluid velocity is non-zero and it can be determined solving the corresponding component of the momentum equation:

$$\frac{\partial^2 u}{\partial y^2} + \frac{\partial^2 u}{\partial z^2} = \frac{1}{\mu}\frac{\partial p}{\partial x} \tag{1}$$

where μ is the dynamic viscosity and p the pressure. Two kind of boundary conditions are needed to solve Eq. (1). The former is the no-slip condition considered at the walls (i.e., $u = 0$). The latter con-

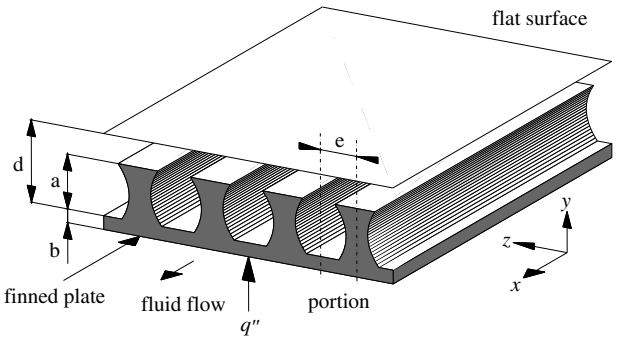

Fig. 1. Finned conduit.

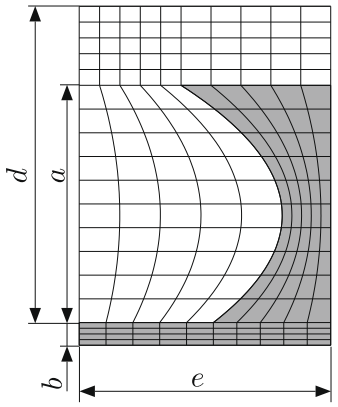

Fig. 2. Computational domain.

sists of the zero velocity partial derivative at the symmetry axes along the normal direction (i.e., $\frac{\partial u}{\partial n} = 0$).

Since the applied heat flux is uniform and the thermal profile is fully developed, the temperatures of the fluid and the solid change linearly with the x coordinate. The conductive heat flux is constant and can be neglected in an overall energy balance. Therefore, the temperature distribution in the coolant is described by the following relationship:

$$\rho c_p u \frac{\partial T_c}{\partial x} = k_c \left[\frac{\partial^2 T_c}{\partial y^2} + \frac{\partial^2 T_c}{\partial z^2} \right] \tag{2}$$

where ρ is the density, c_p the specific heat, and k_c the thermal conductivity of the coolant.

The temperature distribution inside the finned plate is instead described by the Laplace equation:

$$\frac{\partial^2 T_f}{\partial y^2} + \frac{\partial^2 T_f}{\partial z^2} = 0 \tag{3}$$

Eqs. (2) and (3) must be integrated imposing the following boundary conditions:

- on the contact surface, the temperature is the same in the solid and in the fluid;
- on the contact surface, the heat flux in the normal direction is the same in the solid and in the fluid;
- on the symmetry axes and on the insulated wall, the heat flux in the normal direction must be zero;
- on the finned plate bottom surface, the heat flux must be equal to q'' and parallel to the y direction.

Lastly, the value of the temperature in one point of the section is needed.

Eqs. (1)–(3) are here solved numerically by means of the finite element code previously used and tested by Fabbri [9].

In order to evaluate the heat transfer performance of the finned conduit some definitions are given here. For the system described, the following global heat transfer coefficient can be defined as

$$h = \frac{q''}{T_{max} - T_b} \tag{4}$$

where T_{max} is the maximum temperature on the surface on which q'' is imposed and T_b is the bulk temperature of the fluid. The temperatures T_{max} and T_b must be calculated at the same value of the x coordinate. Moreover, it is possible to define an equivalent Nusselt number:

$$Nu_e = \frac{2hd}{k_c} \tag{5}$$

which corresponds to the Nusselt number, which would be calculated if the same heat flux q'' were dissipated through a flat surface with zero thickness at the distance d from the insulated surface.

Moreover, the normalized hydraulic resistance is considered in the optimization:

$$\zeta = \frac{-dp/dx}{w_t/e} \Big/ \frac{12\mu}{d^3} \tag{6}$$

which indicates how many times the hydraulic resistance per unit of length and width of the conduit increases due to the presence of the fins.

Another interesting parameter that can be optimized is the entropy generation through the system which takes into account the irreversibility of the heat transfer and fluid floe processes. Following Bejan [20], the volumetric rate of entropy generation is

$$\dot{S}'''_{gen} = \frac{k}{T^2} \left[\left(\frac{\partial T}{\partial x} \right)^2 + \left(\frac{\partial T}{\partial y} \right)^2 + \left(\frac{\partial T}{\partial z} \right)^2 \right] + \frac{\mu}{T} \Phi \tag{7}$$

where ϕ is the viscous dissipation function. The dimensionless form of Eq. (7) allows to obtained the dimensionless *entropy generation number* as

$$N_S = \bar{S}_{gen} \frac{kT_0^2}{q''^2} \tag{8}$$

where $\bar{S}_{gen}$ is the mean value of the entropy over the conduit section.

The computational domain geometry is described by the parameters a, b, d, e and the fin profile function $g(y)$. Taking d as reference length, we obtain the following dimensionless variables:

$$\alpha = \frac{a}{d}; \quad \beta = \frac{b}{d}; \quad \epsilon = \frac{e}{d}; \quad \phi(\eta) = \frac{g(y)}{d}; \quad \eta = \frac{y}{d} \tag{9}$$

Let us assign a polynomial form to the profile function ϕ:

$$\phi(\eta) = \sum_{i=0}^{n} \psi_i \eta^i \tag{10}$$

the function $\phi(\eta)$ is univocally determined by the $n+1$ parameters ψ_i or, alternatively, by $n+1$ values of ϕ in equidistant points on the η axis, namely:

$$\phi_i = \phi\left(\frac{i}{n} \alpha \right) \tag{11}$$

Since changes in ϕ_i induce in $\phi(\eta)$ variations of more comparable entity then do changes in ψ_i, the first ones are preferable as fin profile describing parameters instead of the latter ones. Moreover, the average half-width of the fin $\bar{\phi}$ results

$$\bar{\phi} = \sum_{i=0}^{n} \frac{\psi_i(\phi_0, \ldots, \phi_n)}{i+1} \alpha^i \tag{12}$$

Hence, we can express the average thickness of the finned plate $\bar{\sigma}$ as

$$\bar{\sigma} = \beta + \frac{\alpha \bar{\phi}}{\epsilon} \tag{13}$$

This parameter is representative of the volume and the weight of the finned plate.

From these definitions, the optimization of a finned plate can be addressed aiming to maximize the Nusselt number and, at the same time, minimizing the hydraulic resistance or minimizing the entropy generated. Moreover, the average thickness can be constrained to an established value $\bar{\sigma}_0$ in order to limit the volume of the fins. To this aim the parameters ϵ and ϕ_i can be reproduced by means of opportune genetic operations whereas, the value of β can be forced to assume the value

$$\beta = \bar{\sigma}_0 - \frac{\alpha}{\epsilon} \bar{\phi} \tag{14}$$

In this way, β can be negative or too small. If that occurs, ϕ_i can be resized or the parameter combination can be rejected by assigning a null value to the Nusselt number and an infinite value to the hydraulic resistance.

3. Multi-objective optimization

To describe a multi-objective optimization let us consider a vector function $\boldsymbol{f}$ which maps a vector variable $\boldsymbol{x}$ of parameters to a vector $\boldsymbol{y}$ of objectives. Formally, the problem of optimizing $\boldsymbol{y}$ can be written as

$$\min / \max \ \boldsymbol{y} = \boldsymbol{f}(\boldsymbol{x}) = (f_1(\boldsymbol{x})), f_2(\boldsymbol{x})), \cdots, f_n(\boldsymbol{x}))) \tag{15}$$

$$\text{subject to } \boldsymbol{g}(\boldsymbol{x}) = (g_1(\boldsymbol{x}), g_2(\boldsymbol{x}), \cdots, g_s(\boldsymbol{x})) \leqslant 0 \tag{16}$$

$$\text{where } \boldsymbol{x} = (x_1, x_2, \ldots, x_m) \in X \tag{17}$$

$$\boldsymbol{y} = (y_1, y_2, \ldots, y_n) \in Y \tag{18}$$

and $\boldsymbol{g}(\boldsymbol{x})$ indicates the constraints that the system is subject to, $\boldsymbol{x}$ is called the *decision vector*, X is the *parameter space*, $\boldsymbol{y}$ is the *objective vector*, and Y is the *objective space*.

A set of decision vectors constitutes a solution to a multicriteria optimization problem if it agrees with the concept of *Pareto optimum* that was formulated by Vilfredo Pareto [13] and it constitutes the basis in multi-objective optimization. In order to explain the concept of Pareto optimality, let us assume, without loss of generality, a maximization problem and let us consider two decision vectors $\boldsymbol{a}, \boldsymbol{b} \in X$. Then, $\boldsymbol{a}$ is said to *dominate* $\boldsymbol{b}$ (according to Zitzler and Thiele [14], written $\boldsymbol{a} \succ \boldsymbol{b}$) if and only if

$$\forall i \in 1,2,\ldots,n : f_i(\boldsymbol{a}) \geqslant f_i(\boldsymbol{b}) \wedge \\ \exists j \in 1,2,\ldots,n : f_j(\boldsymbol{a}) > f_j(\boldsymbol{b}) \tag{19}$$

All decision vectors which are not dominated by any other decision vector of a given set is called *non-dominated* regarding to this set. Whereas, all decision vectors that are non-dominated within the entire search space are denoted as *Pareto optimal* and constitute the so called *Pareto optimal set*. The corresponding objectives instead constitute the *Pareto optimal front* in the objective space.

The two objective functions considered in the present work are the Nusselt number Nu_e and the normalized hydraulic resistance ζ. The first is to be maximized whereas the latter is to be minimized. Following the concept of Pareto optimality, the solutions searched must have the characteristic that it is not possible to increase its Nusselt number without increasing ζ at the same time or, in other words, it is not possible to reduce the normalized hydraulic resistance without decreasing Nu_e at the same time. Furthermore, the parameters ϵ and ϕ_i are the components of the decision vector. Another kind of analysis carried out in the present work consists on the minimization of the entropy generated together the maximization of the heat transfer.

In order to detect the Pareto optimal front, in the present work we used the Strength Pareto Evolutionary Algorithm 2 (SPEA2) developed by Zitzler et al. [15] in 2001. The algorithm starts with an initial population $\boldsymbol{P}$ of N individuals, and create an external empty set $\bar{\boldsymbol{P}}$. At each generation t, the value of a function $F(i)$ called fitness is computed (cf. Section 3.1) for each element in $\boldsymbol{P}_t$ and $\bar{\boldsymbol{P}}_t$. Thereafter, all non-dominated individuals in $\boldsymbol{P}_t$ and $\bar{\boldsymbol{P}}_t$ are copied to the external archive of the subsequent generation $\bar{\boldsymbol{P}}_{t+1}$. If the number of elements in $\bar{\boldsymbol{P}}_{t+1}$ exceeds its maximum allowed size $\bar{N}$, $\bar{\boldsymbol{P}}_{t+1}$ is reduced by means of a truncation operator. Otherwise, if the size of $\bar{\boldsymbol{P}}_{t+1}$ is less than $\bar{N}$, then $\bar{\boldsymbol{P}}_{t+1}$ is filled with the dominated solution with lower value of $F(i)$. The external population is then let to reproduce (cf. Section 3.2) in order to have a new population to evaluate and the algorithm continues until a stopping criteria is satisfied.

Since the fitness value will be important to understand the genetic operators employed here, it is deeply recalled in the following whereas the reader can have an exhaustive explanation of the truncation operator in the original paper of Zitzler et al. However, it is worth noting that the main feature of the truncation operator consists in eliminating solutions that are too close to others without removing boundary elements of the Pareto front (i.e., global optima) and it allows to obtain well sampled fronts.

3.1. Fitness assignment

In order to compute the fitness, three values for each individual i must be first calculated: the strength $S(i)$, the raw fitness $R(i)$ and the density $D(i)$. Firstly, Zitzler and Thiele [14] define the strength of the ith individual $S(i)$ as the number of solutions it dominates:

$$S(i) = |\{j | j \in \boldsymbol{P}_t + \bar{\boldsymbol{P}}_t \wedge i \succ j\}| \tag{20}$$

where $|\cdot|$ indicates the cardinality of the set, $+$ stands for the multiset union and the symbol $\succ$ corresponds to the Pareto dominance relation. Once the strength is evaluated, the value of the raw fitness of the individual i can be computed as the sum of the strengths of its dominators:

$$R(i) = \sum_{j \in \boldsymbol{P}_t + \bar{\boldsymbol{P}}_t, j \succ i} S(j) \tag{21}$$

In order to illustrate how the strength and the raw fitness assignment works, in Fig. 3 these values are reported close to each element of a population. The problem depicted consists in maximizing both the cost function f_1 and the cost function f_2.

Since elements lying near the Pareto front should be more probably preferred during reproduction, then elements with lower raw fitness values will be chosen with a higher probability than individuals with higher values of $R(i)$. However, further information must be also included in order to discriminate between individuals with the same values of R. This can be done including information about individual density in the objective space to the raw fitness value. The density estimation technique provided in SPEA2 by Zitzler and Thiele [14] consists in an adaption of the kth nearest neighbor method [16]. In particular, for each element i the distance between it and all the other individuals in the objective space is stored in a list. After having sorted this list in ascending order, the kth distance σ_k^i is chosen. The value of k is equal to the square root of the sample size:

$$k = \sqrt{N + \bar{N}} \tag{22}$$

The density of the ith individual is then defined by the following relation

$$D(i) = \frac{1}{\sigma_i^k + 2} \tag{23}$$

Finally, the fitness value of the ith individual can be computed as

$$F(i) = R(i) + D(i) \tag{24}$$

When the algorithm copies the non-dominated solution to the external archive, it chooses the elements with value of fitness lower than one. If the number of non-dominated individuals is lower than the maximum number of external elements, then the archive is filled by means of dominated individuals with the lower value of fitness. By the definition of Zitzler and Thiele [14], the fitness function of an element will always be grater than zero and the lower the value of the fitness the better will be the corresponding individual.

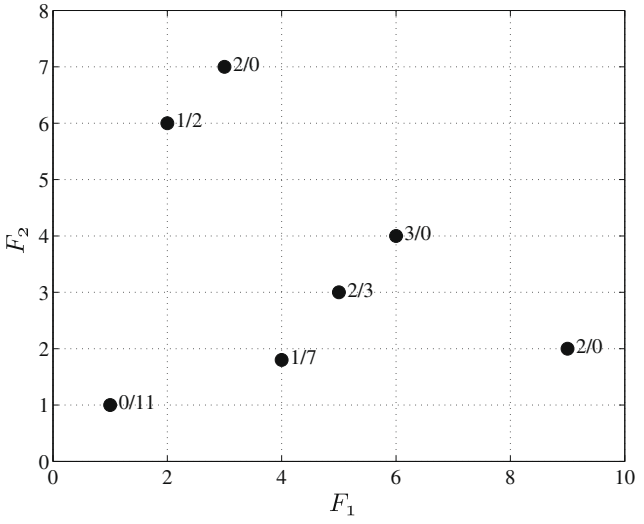

Fig. 3. Strength $S(i)$ and raw $R(i)$ fitness assignment of the SPEA 2. Both F_1 and F_2 are to be maximized. Points are plotted with $S(i)/R(i)$ near the ith individual.

Moreover, the fitness value is important to select elements for the reproduction and, in the present work, it is used also in the reproduction process itself as described in the following.

3.2. Mating scheme and genetic operators

In order to create a new population to evaluate, two individuals are selected from the external population. The element with the lower value of the fitness is then chosen as the first parent. The second parent is selected similarly as the previous one.

Once the two parents are selected, they are removed from the external population and they generate two offspring. The way that two parents reproduce themselves is a key issue in a genetic algorithm. The crossover here used is based on concept that information provided by the SPEA2 about density and dominance of individuals can be employed in order to search in regions of the objective space that have been poorly investigated by the algorithm in previous generations. To illustrate how this genetic operator works, let us consider two parents $\boldsymbol{P}_1$ and $\boldsymbol{P}_2$ with fitness values F_1 and F_2, respectively. Moreover, let us assume that F_1 is lower than F_2 and that both F_1 and F_2 are less than zero (i.e., both $\boldsymbol{P}_1$ and $\boldsymbol{P}_2$ are on a Pareto front). This means that $\boldsymbol{P}_1$ belongs to a region less crowded than the region of $\boldsymbol{P}_2$. In such a case, the genetic algorithm is preferred to investigate closer to $\boldsymbol{P}_1$ rather than $\boldsymbol{P}_2$. In the case that F_2 is greater than one, once again the genetic algorithm should search closer to $\boldsymbol{P}_1$ than to $\boldsymbol{P}_2$. Moreover, the reproduction process should not only take into account if one of the fitness is lower than the other, but it should also consider how much these two values are different one to each other. To this aim, each couple of parents simply generates two offspring ($\boldsymbol{o}_1$ and $\boldsymbol{o}_2$) in the following way:

$$\vec{o}_1 = \lambda\left(\frac{F_2}{F_1}\vec{P}_1 + \frac{F_1}{F_2}\vec{P}_2\right) \tag{25}$$

$$\vec{o}_2 = \lambda\left(\frac{F_2}{F_1}\vec{P}_1 - \frac{F_1}{F_2}\vec{P}_2\right) \tag{26}$$

where λ is a random number between [0, 1] and it has been assumed that $F_1 < F_2$. The generated offspring together their parents are shown in Fig. 4 and considering that individuals have a number of two variables (x and y). Moreover, in the present work a floating-point representation of individuals has been considered.

Lastly, in order to avoid the genetic algorithm to stuck on sub-optimal Pareto fronts (or in local optima when considering single objective optimization) the routine is forced to investigate other regions of the objective space by means of a mutation operator. The mutation operator used in the present work consists in random changes in some components of a certain percentage of the decision vectors of the external population.

4. Test function: the Poloni test case

The SPEA2 has been tested on many mathematical problems. All the test cases reported in [17] and in [18] have been successfully solved. However, we here report only the results regarding the Poloni test case since it demonstrated to be the hardest to solve.

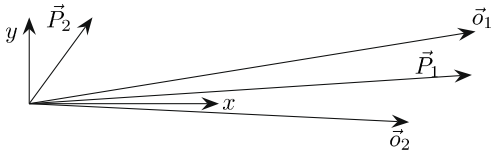

Fig. 4. Offsprings $\vec{o}_1$ and $\vec{o}_2$ generated by two parents $\vec{P}_1$ and $\vec{P}_2$ in the case of F_1 lower than F_2.

The problem here presented consists in minimizing the following functions:

$$t_1(x,y) = 1 + (a-b)^2 + (c-d)^2 \tag{27}$$

$$t_2(x,y) = (x+3)^2 + (y+1)^2 \tag{28}$$

where

$$x, y \in [-\pi, \pi] \tag{29}$$

and the parameters presented in F_1 are

$$a = 0.5sin(1) - 2.0cos(1) + 1.0sin(2) - 1.5cos(2) \tag{30}$$
$$b = 0.5sin(x) - 2.0cos(x) + 1.0sin(y) - 1.5cos(y) \tag{31}$$
$$c = 1.5sin(1) - 1.0cos(1) + 2.0sin(2) - 0.5cos(2) \tag{32}$$
$$d = 1.5sin(x) - 1.0cos(x) + 2.0sin(y) - 0.5cos(y) \tag{33}$$

Fig. 5 shows the objective space obtained by sampling each of the variables x and y by means of 64 uniformly spaced points (corresponding to a grid of 64×64 points).

In order to face a more significant test, the two variables are divided into nine components as follows:

$$x_i, y_j \in \left[-\frac{\pi}{9}, \frac{\pi}{9}\right] \tag{34}$$

$$x = \sum_{i=1}^{9} x_i \tag{35}$$

$$y = \sum_{j=1}^{9} y_j \tag{36}$$

The resulting dimension of the optimization problem is of 18 variables and two objectives. In the case analyzed here, we have tested all the genetic operators previously described and considering several runs of the genetic algorithm. A population size of 100 individuals and an external population of 50 individuals has been chosen. Moreover, a mutation probability of the 5% has been selected. In Fig. 6 the *sampled* real Pareto front is depicted together with the Pareto front detected by the SPEA2 considering a population of 100 individuals, an external population of 50 individuals, and running for 100 generations. Fig. 7 shows the mean convergence history obtained in 50 runs of the SPEA2 with randomly generated starting populations. The convergence has been computed considering the convergence metric $C(\boldsymbol{P})$ suggested by Deb and Jain

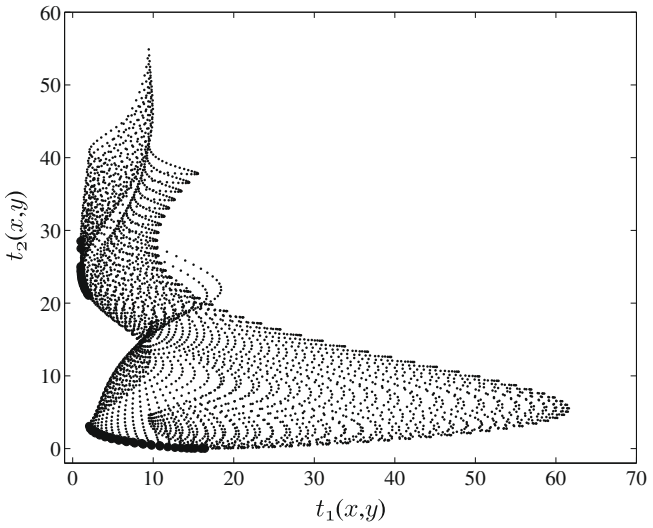

Fig. 5. 64×64 sampling of the objective function in the objective space. (Points marked with • correspond to the Pareto front).

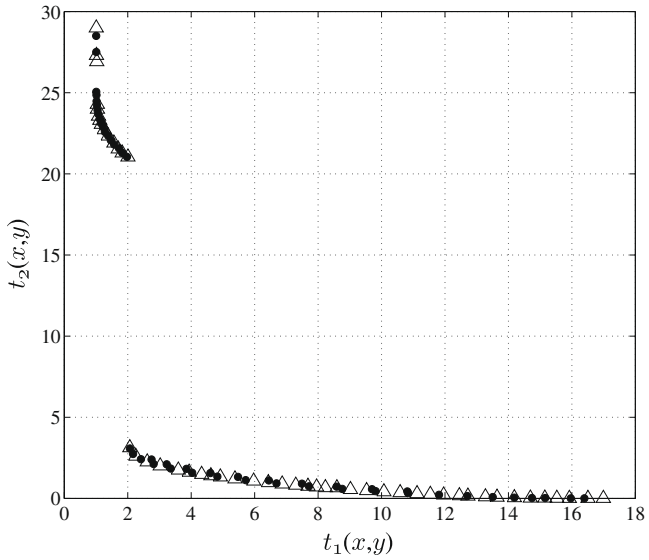

Fig. 6. Approximated Pareto front obtained running SPEA2 with 100 individuals, 50 external individuals, and for 100 generations. (•) Sampled Pareto front; (△) Pareto front detected by SPEA2.

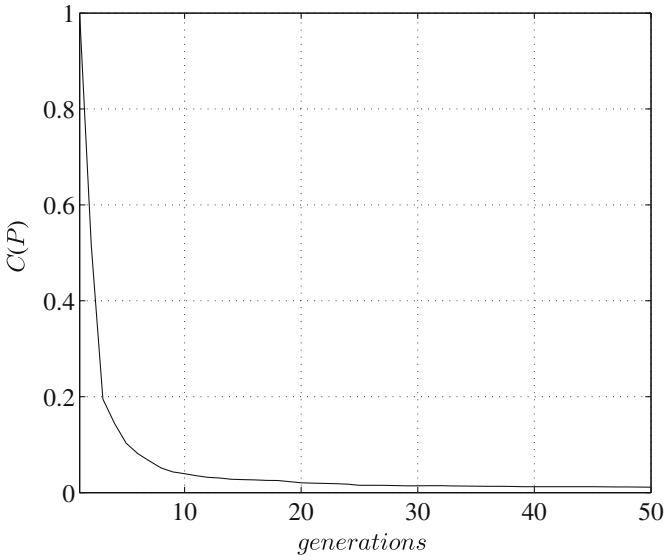

Fig. 7. Mean convergence history of the SPEA2 used in the Poloni test problem obtained in 50 runs.

[19], which measures the average Euclidean distance between an approximation set and a reference set (i.e., the sampled Pareto front). Such a metric is equal to zero only when the non-dominated elements exactly match the reference points which is almost impossible. For this reason in Fig. 7 the metric do not reaches the null value within 50 generations. However, it can be seen that the algorithm employed is particularly fast in finding the Pareto front of the test case presented.

5. Results

The SPEA2 algorithm has been employed to optimize the geometry previously studied by Fabbri [10]. Only three values of the polynomial order n of the fin profile function have been studied here, namely

$$n = 0, 2, 4 \tag{37}$$

The parameters set up of the algorithm used to optimize the fins is listed below:

- population size, $= 100$;
- external population size, $\bar{P} = 50$;
- maximum number of generation, $t_{max} = 100$.

For the finite element method, a grid with 20×80 elements (21×81 nodes) was used. More finer grids have been tested without finding any significant variation in Nu_e. In the test cases, a grid of 35×80 elements caused changes in Nu_e of less than 0.5% whereas, a grid of 20×110 elements produced alterations in Nu_e of less than 0.7%. Moreover, the normalized fin height α has been considered equal to 0.75 and the thermal conductivity ratio γ equal to 300. Such a value of γ corresponds to the case of a copper finned plate cooled by water. The remaining geometrical parameters has been allowed to vary between the following values:

$$0.001 \leqslant \beta \leqslant 0.2 \tag{38}$$

$$0.05 \leqslant \epsilon \leqslant 0.6 \tag{39}$$

$$0.001 \leqslant \phi_i \leqslant \epsilon \tag{40}$$

In Table 1, parameters on the left of the vertical line have been imposed, while those on the right have been found by the genetic optimization algorithm.

5.1. Optimization without constraints

Fig. 8 shows the Pareto fronts related to the three cases here analyzed. It can be seen that for all the polynomial orders considered, the maximum Nusselt Number agrees with data reported by Fabbri [10]. Moreover, all the cases tested has detected the Pareto front in much fewer generations than t_{max}. In particular, the 4th polynomial order has been the most complex to solve since the resulting number of variables was equal to seven. In that case, the Pareto front has been detected and well sampled within 40 generations. Whereas, the rectangular fin shape and the parabolic fin profile have been solved within 20 and 30 generations, respectively. The analysis has been limited to the detection of the maximum Nusselt number since

Table 1
Geometries that ensure a reduction of about 20% of the hydraulic resistance of maximum heat transfer geometries.

α	n	$\bar{\sigma}$	β	ϵ	ϕ_0	ϕ_1	ϕ_2	ϕ_3	ϕ_4	Nu_e	ζ	$\Delta Nu_e(\%)$	$\Delta\zeta(\%)$
0.75	0	0.256	0.0861	0.2085	0.0472	–	–	–	–	57.66	12.31	4.1	23
0.75	2	0.322	0.1304	0.2036	0.0815	0.0272	0.1225	–	–	77.46	15.50	5.8	24
0.75	4	0.276	0.1043	0.1958	0.0915	0.0375	0.0322	0.0254	0.1426	82.93	16.00	4.7	20
0.75	0	0.200	0.0710	0.1923	0.0331	–	–	–	–	56.03	11.96	4.5	22
0.75	2	0.200	0.0380	0.1982	0.0751	0.0191	0.1055	–	–	72.50	14.31	5.6	23
0.75	4	0.200	0.0472	0.1978	0.0943	0.0337	0.0350	0.0152	0.1405	79.97	15.17	6.7	23
0.75	0	0.100	0.0244	0.1805	0.0182	–	–	–	–	48.80	10.83	4	21
0.75	2	0.100	0.0144	0.1874	0.0371	0.0118	0.04	–	–	52.70	11.04	5	23
0.75	4	0.100	0.0158	0.1855	0.0469	0.0129	0.0143	0.0103	0.0903	59.74	12.37	5.3	22

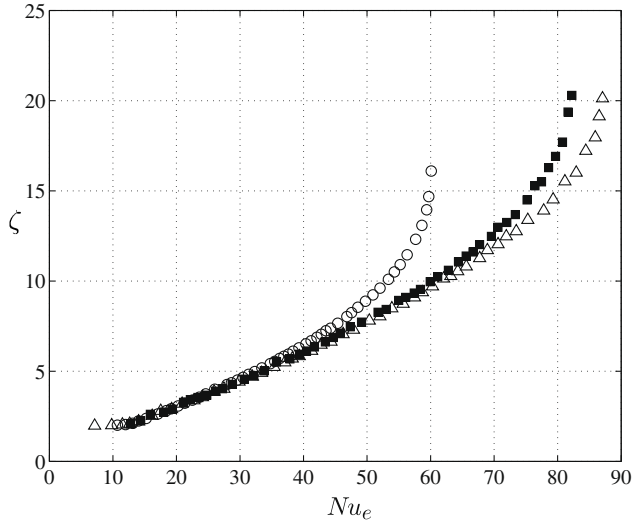

Fig. 8. Pareto fronts of the unconstrained cases. (○) Rectangular fins, (■) parabolic fins, (△) 4th order fins.

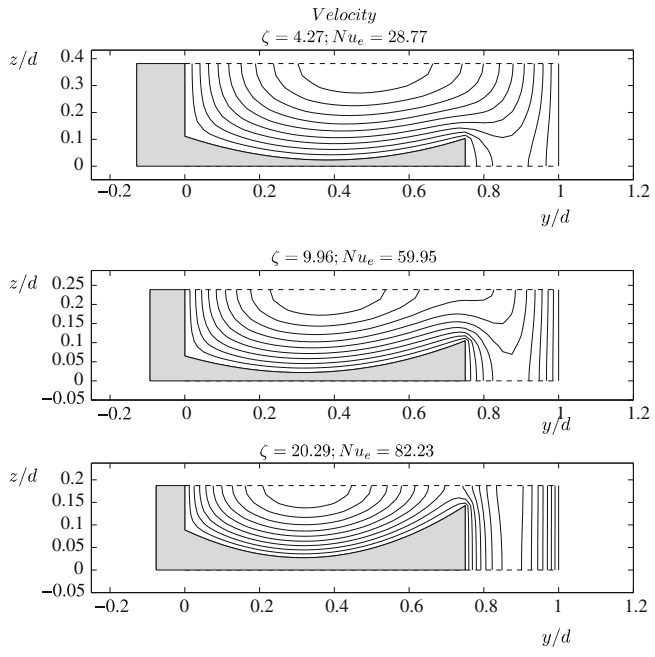

Fig. 9. Velocity distributions in the transversal section for $n = 2$, $\alpha = 0.75$. Curves are drawn every 10% of the maximum velocity.

Fabbri [10] demonstrated that those geometries that maximize the fin efficiency also maximize Nu_e. Therefore, the fin efficiency has not been considered here.

A first important consideration that can be made on the basis of the present results concerns with global optimum geometries. In fact, it can be clearly seen that there are profiles that provide good performance in terms of heat exchange but, at the same time, are also able to provide a sensible reduction of the hydraulic resistance. In Table 1, profiles that provide the maximum heat transfer with a reduction of the hydraulic resistance of at least the 20% are listed. For all the unconstrained geometries, the Nusselt number decrease ranges between 4.1% and 5.8% whereas, the ζ has a reduction that ranges between 20% and 24%.

If it is of interest the maximum heat transfer, Fabbri [10] pointed out that optimum geometries are based on a compromise between two exigencies. The first consists in having, in the cavities between the fins, velocities which are comparable with those at fin tip or higher. In fact, higher velocity near the fin tip causes higher thermal gradients in this region, which would lower the bulk temperature without enhancing the heat transfer from the plate base and the lateral surface on the fin. The second exigence consists in maintaining the maximum velocity as close to the dissipator as possible in order to relatively increase the thermal gradient. As a consequence of the first exigence, fins cannot be too closely spaced, for the second one they cannot be too sparse. When dealing with Pareto optimal solutions, the balance between the two exigencies progressively change. In particular, since here we are interested in minimizing the hydraulic resistance, the individuals belonging to the Pareto front exhibit the tendency of having larger cavities

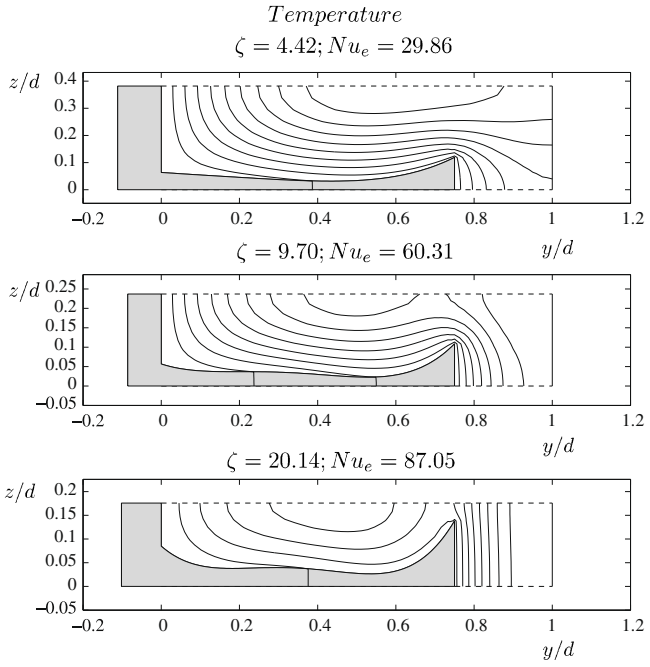

Fig. 10. Temperature distributions in the transversal section for $n = 4$, $\alpha = 0.75$. Curves are drawn every 10% of the difference between the maximum and the minimum temperature.

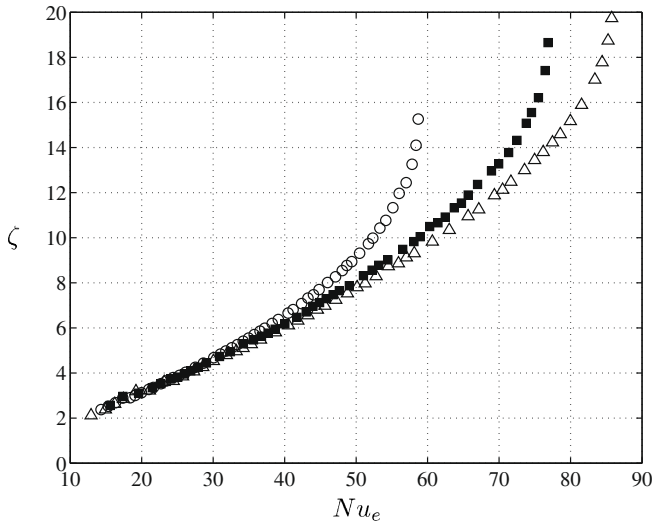

Fig. 11. Pareto fronts in case of constrained solid volume $\bar{\sigma}_0 = 0.2$. (○) Rectangular fins, (■) parabolic fins, (△) 4th order fins.

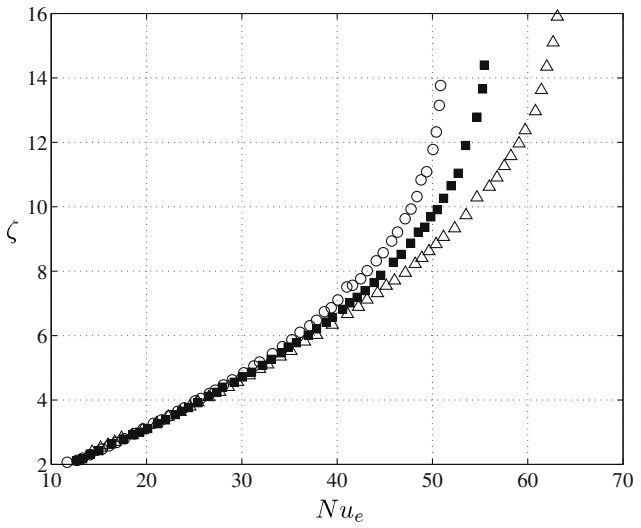

Fig. 12. Pareto fronts in case of constrained solid volume $\bar{\sigma}_0 = 0.1$. (○) Rectangular fins, (■) parabolic fins, (△) 4th order fins.

between the fins as the parameter ζ decreases. This can be deduced from Fig. 13 where four cases belonging to the Pareto front of $n = 4$ are depicted. From this figure, it can be seen that the fin spacing progressively decreases as the Nusselt number increases. Also the fin profile changes since the fin tip tends to extend toward the center of the channel between the fins. In fact, higher order profiles that maximize the Nusselt number force the maximum velocity to occur between the fins. Such a behavior induces higher thermal gradients near the finned plate base and the fin lateral surface. At low hydraulic resistance, the fin tips are thinner and the maximum velocity progressively occurs at higher values of the normalized coordinate η (see Fig. 9) . As consequence of having thinner fin tips and larger cavities, the performance of wavy fins are not much different from those obtained with rectangular fins and the Pareto fronts overlap at low ζ. In other words, if a designer is interested in cases where the constraint imposed in ζ is particularly stringent, the employment of corrugated fins is not useful to improve the heat transfer coefficient. Such an effect can be clearly seen in Fig. 8 where the curves related to the geometries analyzed here overlap if $\zeta < 6$. Moreover, parabolic and 4th order fins provide similar performance if $\zeta \lesssim 10$. This is of fundamental role if also manufacturing exigencies are taken into account since rectangular fins are easier to realize. On the other hand, complex fin profiles are more expensive to realize than rectangular devices but the manufacturing cost of these complex fins can be easily gained thanks to lower usage costs (Fig. 10).

5.2. Optimization with constrained volume

In practice, in the optimization of a particular geometry, some constraints may also arise. In the application presented here, a typical constraint can be the solid volume of the device. In the present analysis, we set up two different values of the average thickness of the finned plate, namely $\bar{\sigma}_0 = 0.2$ and $\bar{\sigma}_0 = 0.1$.

Figs. 11 and 12 show the Pareto fronts for the two limits considered and for the three geometries optimized here. In all cases the constraint entail a reduction of the heat transfer as already pointed

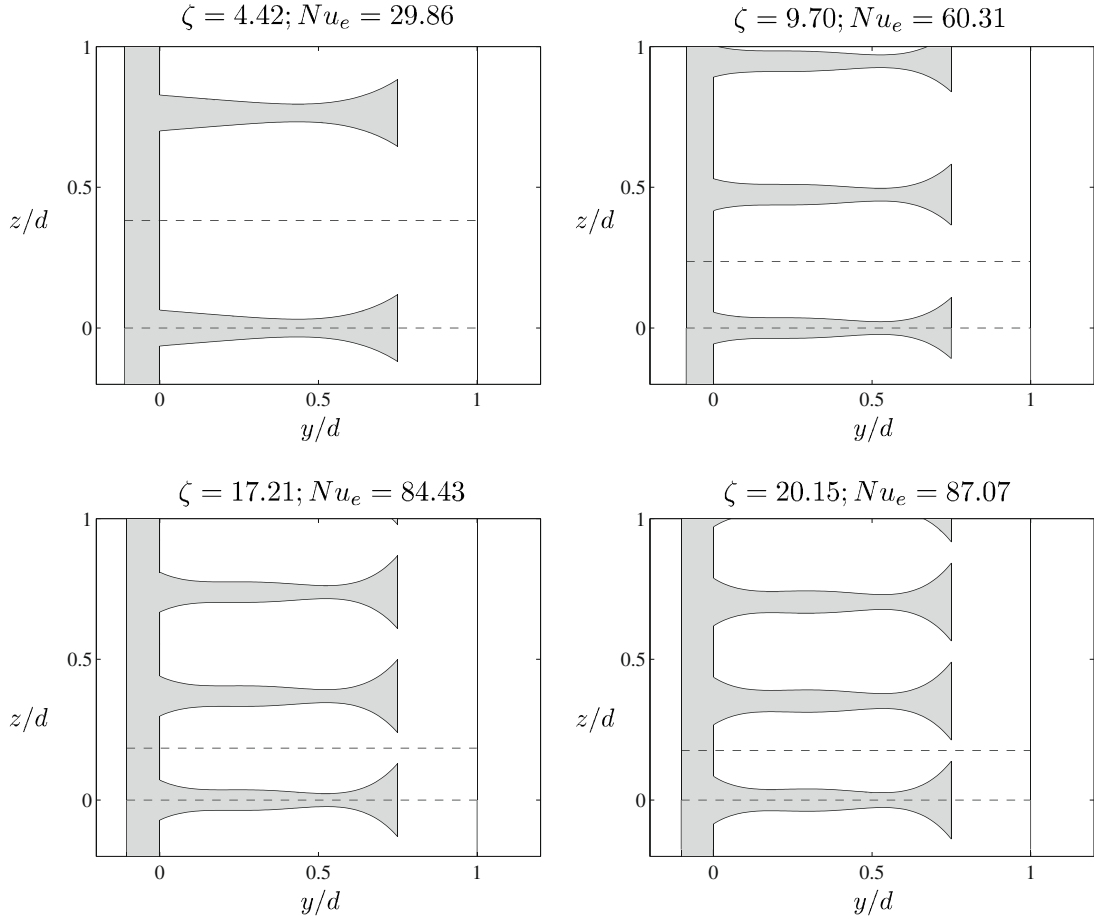

Fig. 13. Optimum geometries for $n = 4$.

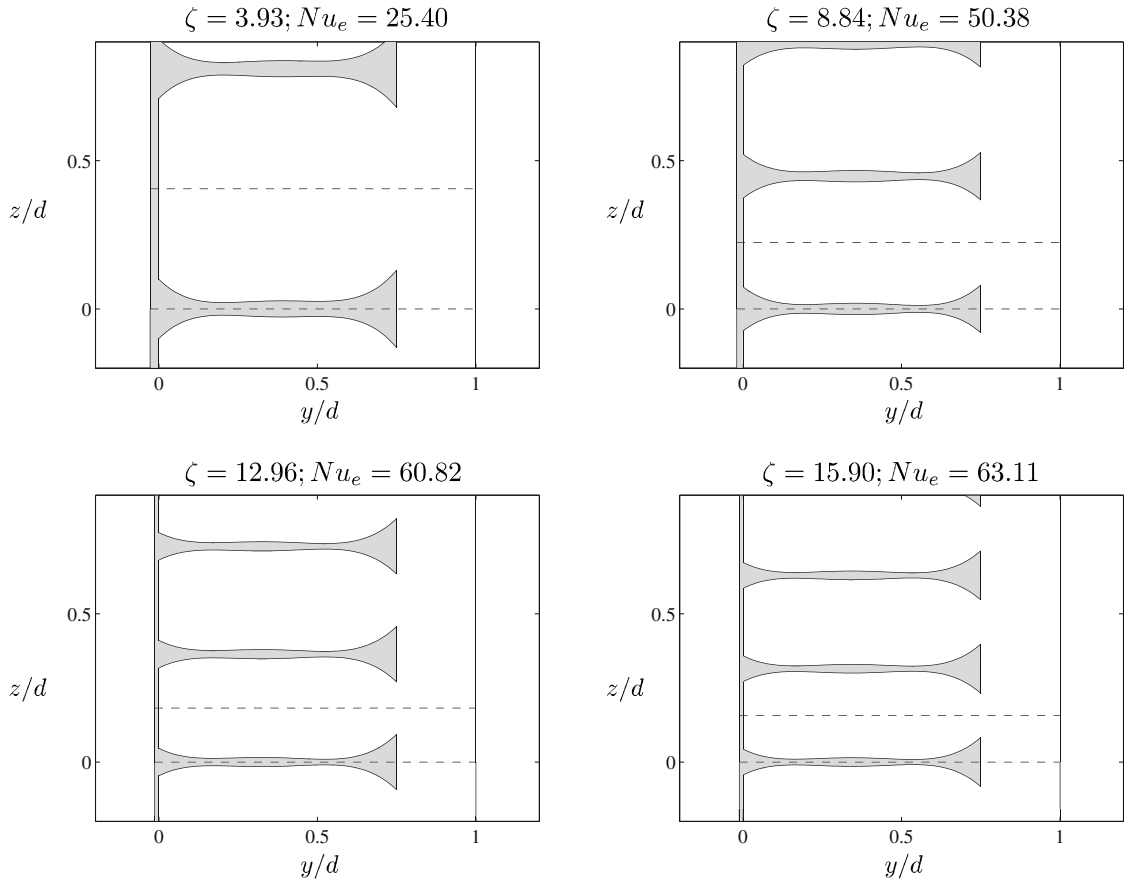

Fig. 14. Optimum geometries for $n = 4$ with a constrained solid volume $\bar{\sigma}_0 = 0.1$.

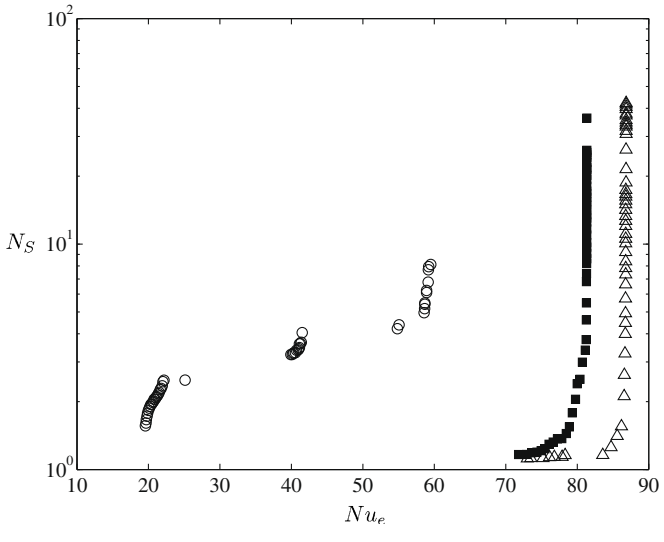

Fig. 15. Pareto fronts for the optimization of the entropy generation. (○) Rectangular fins, (■) parabolic fins, (△) 4th order fins.

out by Fabbri [10]. However, the same consideration of the unconstrained study can sentenced be here. In fact, in all cases there are geometries that provide good performances in terms of heat transfer and, at the same time, provide a significant reduction of the parameter ζ (see Table 1). Moreover, in all cases, constrained and unconstrained, the three Pareto front overlap when Nu_e is lower than 40.

5.3. Optimization of the entropy generation

Another interesting parameter to be minimized together the maximization of the heat transfer is the entropy generated. Specifically, the parameter optimized is the entropy generation number (see Eq. 8). Geometries with lower N_S and higher Nu_e are thermodynamically advantageous since in addition to enhancing the heat transfer they reduce the irreversibility of the apparatus (Fig. 14).

Fig. 15 reports the Pareto fronts of the three type of profiles. It can be seen that, for the parabolic and the 4th order polynomial fins, a large reduction of N_S is present if Nu_e decreases. Moreover, for this type of parametrization, no solution is detected by the genetic algorithm for values of the Nusselt number lower than about 70. This is due to the fact that geometries with low heat transfer characteristics have also higher values of N_S. Therefore, they are dominated solutions and they do not belong to the Pareto front. The optimal frontier of rectangular fins is more complex than other cases and the entropy generated varies in a non-trivial way as the Nusselt number decreases. Finally, the analysis of geometries laying on the Pareto-front allows similar considerations that has been formulated in the optimization of the pressure drop and the Nusselt number (i.e., the fin spacing decreases with an increment of Nu_e, as the Nusselt number decreases the fin tips become thinner, etc.).

6. Conclusions

In the present work we applied the multi-objective approach to the optimization of the heat transfer through finned heat dissipator cooled by laminar flow. In particular we studied the optimal geom-

etry of wavy fins described by polynomial functions and we searched the parameter combinations that aim to maximize the heat transfer and, at the same time, aim to minimize the hydraulic resistance. The results are a set of solutions lying on a curve called Pareto front and the analysis of this curve allows to find geometries where the Nusselt number is slightly reduced but the hydraulic resistance is appreciably lower than the one computed in the best heat exchanger profile. Moreover, if the hydraulic resistance is limited to a particular stringent value, the adoption of wavy fins do not improve the heat transfer of the device here analyzed.

In the present work we also studied the effect of a constrained solid volume of the fins. The main effect, as expected, consists in a reduction of the heat transfer. As in the unconstrained case, there are geometries that provide a great reduction of the hydraulic resistance without reducing the heat transfer.

It must also be remarked that the present analysis has been limited to cases where the fluid flow has been considered laminar and fully developed. Therefore, the results presented here can be usefully employed only in cases where the entrance region is short in respect to the total length and where the Reynolds number is low.

Lastly, some remarks should be made regarding to the optimization process. The configuration of the SPEA2 employed here can be too computationally expensive if applied to more complex problems such as three-dimensional cases. Therefore, if the simulation time of the single individual is relevant, the parallelization of the genetic algorithm and the adoption of hybrid techniques can significantly speed up the optimization process.

References

[1] LCA (Life Cycle Assessment Committee Report), Summary of Inventory Data, Japan Aluminium Association, 1999.
[2] A. Bar-Cohen, M. Iyengar, Design and optimization of air-cooled heat sinks for sustainable development, IEEE Trans. Components Pack. Technol. 25 (4) (2002) 584–591.
[3] A.D. Snider, A.D. Kraus, The quest for the optimum longitudinal fin profile, Heat Transfer Eng. 8 (1987) 19–25.
[4] A.D. Snider, A.D. Kraus, S. Graff, M. Rodriguez, A.G. Kusmierczyk, Optimal fin profiles. Classical and modern, in: Proceedings of the Ninth International Conference on Heat Transfer, 1990, pp. 15–19.
[5] R.J. Duffin, A variational problem relating to cooling fins, J. Math. Mech. 8 (1959) 47–56.
[6] C.J. Maday, The minimum weight one-dimensional straight fin, ASME J. Eng. Ind. 96 (1974) 161–165.
[7] M. Spiga, G. Fabbri, Effcienza di dissipatori a profilo sinusoidale, in: Proceedings of the 12th UIT National Congress, L'Aquila, Italy, 1994, pp. 197–204.
[8] G. Fabbri, G. Lorenzini, Analisi numerica bidimensionale di dissipatori a profilo sinusoidale, in: Proceedings of the 13th UIT National Congress, Bologna, Italy, 1995, pp. 491–499.
[9] G. Fabbri, A genetic algorithm for fin profile optimization, Int. J. Heat Mass Transfer 40 (1997) 2165–2172.
[10] G. Fabbri, Optimization of heat transfer through finned dissipators cooled by laminar flow, Int. J. Heat Fluid Flow 19 (1998) 644–654.
[11] R. Hilbert, G. Janiga, R. Baron, D. Thévenin, Multi-objective shape optimization of a heat exchanger using parallel genetic algorithms, Int. J. Heat Mass Transfer 49 (2006) 2567–2577.
[12] E. Nobile, F. Pinto, G. Rizzetto, Geometric parametrization and multi-objective shape optimization of convective periodic channels, Numer. Heat Transfer B 50 (2006) 425–453.
[13] Vilfredo Pareto, Cours D'économie politique, F. Rouge, 1896.
[14] E. Zitzler, L. Thiele, Multiobjective evolutionary algorithms: a comparative case study and the strength Pareto approach, IEEE Trans. Evol. Comput. 3 (1999) 257–271.
[15] E. Zitzler, M. Laumanns, L. Thiele, SPEA2: Improving the Strength Pareto Evolutionary Algorithm, Computer Engineering and Networks Laboratory, ETH Zurich, 2001.
[16] B.W. Silverman, Density Estimation for Statistics and Data Analysis, Chapman and Hall, London, 1986.
[17] K. Deb, S. Agrawal, A. Pratab, T. Meyarivan, A fast elitist non-dominated sorting genetic algorithm for multi-objective optimization: NSGA-II, in: Proceedings of the Parallel Problem Solving from Nature VI Conference, Springer. Lecture Notes in Computer Science No. 1917, Paris, France, 2000, pp. 849–858.
[18] E. Rigoni, Hole Functions Problem, ESTECO Technical Report 2004-003, 2004. Available from: <http://www.esteco.com>.
[19] K. Deb, S. Jain, Running Performance Metrics for Evolutionary Multi-Objective Optimization, Indian Institute of Technology, Technical Report 2002004, 2002.
[20] A. Bejan, Entropy Generation Through Heat and Fluid Flow, Wiley, New York, 1982.